RESEARCH ARTICLE

# Graphene Oxide Induces Ester Bonds Hydrolysis of Poly-l-lactic Acid Scaffold to Accelerate Degradation

**Cijun Shuai[1,2,3], Yang Li[1], Wenjing Yang[1], Li Yu[1], Youwen Yang[2], Shuping Peng[4,5], Pei Feng[1]***

[1]State Key Laboratory of High-Performance Complex Manufacturing, College of Mechanical and Electrical Engineering, Central South University, Changsha 410083, China

[2]Institute of Bioadditive Manufacturing, Jiangxi University of Science and Technology, Nanchang 330013, China

[3]Shenzhen Institute of Information Technology, Shenzhen 518172, China

[4]NHC Key Laboratory of Carcinogenesis and The Key Laboratory of Carcinogenesis and Cancer Invasion of the Chinese Ministry of Education, Xiangya Hospital, Central South University, Changsha, Hunan China

[5]Cancer Research Institute, School of Basic Medical Sciences, Central South University, Changsha, Hunan China

**Abstract:** Poly-l-lactic acid (PLLA) possesses good biocompatibility and bioabsorbability as scaffold material, while slow degradation rate limits its application in bone tissue engineering. In this study, graphene oxide (GO) was introduced into the PLLA scaffold prepared by selective laser sintering to accelerate degradation. The reason was that GO with a large number of oxygen-containing functional groups attracted water molecules and transported them into scaffold through the interface microchannels formed between lamellar GO and PLLA matrix. More importantly, hydrogen bonding interaction between the functional groups of GO and the ester bonds of PLLA induced the ester bonds to deflect toward the interfaces, making water molecules attack the ester bonds and thereby breaking the molecular chain of PLLA to accelerate degradation. As a result, some micropores appeared on the surface of the PLLA scaffold, and mass loss was increased from 0.81% to 4.22% after immersing for 4 weeks when 0.9% GO was introduced. Besides, the tensile strength and compressive strength of the scaffolds increased by 24.3% and 137.4%, respectively, due to the reinforced effect of GO. In addition, the scaffold also demonstrated good bioactivity and cytocompatibility.

**Keywords:** Poly-l-lactic acid scaffold, GO, Degradation property, Ester bonds hydrolysis

***Corresponding Author:** Pei Feng, State Key Laboratory of High-Performance Complex Manufacturing, College of Mechanical and Electrical Engineering, Central South University, Changsha 410083, China; fengpei@csu.edu.cn

***Received:*** November 15, 2019; ***Accepted:*** January 02, 2020; ***Published Online:*** January 23, 2020

**Citation:** Shuai C, Li Y, Yang W, *et al*., 2020, Graphene oxide induces ester bonds hydrolysis of poly-l-lactic acid scaffold to accelerate degradation. *Int J Bioprint*, 6(1):249. DOI: 10.18063/ijb.v6i1.249

## 1 Introduction

Poly-l-lactic acid (PLLA) is a bone scaffold material[1,2], recognized by the US Food and Drug Administration (FDA) with good biocompatibility and bioabsorbability[3,4]. It can be first degraded into lactic acid in the human body, then decomposed into carbon dioxide and water by metabolism, and finally excreted without any harmful residue[5-7]. In addition, the elastic modulus of PLLA is close to that of human bone tissue compared to stainless steel, titanium alloy, etc., and can avoid stress shielding effect[8-10] whereas the degradation rate of PLLA is slow in the human body. It has been reported that PLLA needs a complete resorption time of 2 – 3 years[11], while new bone regeneration[12-14], usually takes 12 – 18 weeks[15]. The unmatched degradation rate of PLLA with new bone regeneration limits its further applications.

To accelerate the degradation of PLLA, Kang *et al*. blended collagen and PLLA, using collagen's natural fast degradability to accelerate degradation. Nevertheless, the introduction of collagen decreased the mechanical strength of the PLLA scaffold[16]. Considering that PLLA is formed by the linkage of ester bonds between lactic acid monomers, its degradation is first caused by the hydrolysis of the ester bond in the main chains and then decomposes into carbon dioxide and water[17]. PLLA is a hydrophobic material and is not beneficial for the intrusion of water molecules into its interior to break the ester bonds, making it difficult to degrade[18]. Therefore, promoting the contact between water molecules and the ester bond of PLLA is an effective method to accelerate the hydrolysis of ester bonds.

Graphene oxide (GO) is a two-dimensional lamellar structure with a large amount of oxygen-containing functional groups (such as –COOH and –OH) on its surface[19-22]. These functional groups can endow GO good hydrophilic property and water absorption capacity[23-26]. At the same time, the lamellar GO with large surface area is likely to form many interfaces with matrix, and these interfaces can be regarded as microchannels to facilitate water molecules to invade and induce the breaking of ester bonds. Besides, GO with excellent mechanical properties (Young's modulus >0.5 TPa, and tensile strength ~130 GPa) can be used as a reinforcing phase for scaffold[27,28]. In addition, it has also been reported that GO possessed good biocompatibility for cell adhesion and proliferation[29-31]. The current reports mainly utilized GO to improve the mechanical properties, thermal stability, and cytocompatibility of PLLA[32-35] whereas few studies focused on inducing ester bonds hydrolysis of PLLA scaffold by GO to accelerate degradation.

In this study, GO was introduced into PLLA to accelerate degradation, and three-dimensional porous PLLA/GO scaffolds were prepared by selective laser sintering (SLS)[36], which is an additive manufacturing method[37], and can realize the preparation of personalized scaffolds and interconnected porous structures compared to traditional fabrication methods[38-42]. Degradation properties of the PLLA scaffold containing different ratios of GO were studied by observation of degradation morphology and measurement of mass loss. Meanwhile, degradation mechanism was also analyzed. Besides, surface and fracture morphologies of the scaffold were also observed to further investigate the causes of changes in mechanical properties. In addition, bioactivity and cytocompatibility had also been evaluated by simulated body fluid (SBF) immersion and cell proliferation experiments, respectively.

## 2 Materials and methods

### 2.1 Materials and preparation

PLLA powders (Purity: tionigand inherent viscosity: 1.46 dl/g) were provided from Shenzhen Polymtek Biomaterial Co., Ltd. (Shenzhen, China). GO powders (purity > 98%) were obtained from Chengdu Organic Chemicals Co., Ltd. (Chengdu, China). The composition of phosphate-buffered solution (PBS) was NaCl, KCl, $Na_2HPO2H_2O$, and $KH_2PO_4$, which was provided from Sigma-Aldrich (Beijing, China). SBF was purchased from Qingdao Jieshang Biological Technology Co., Ltd. (Qingdao, China). Human osteoblast-like MG-63 cells were supplied from the American Type Culture Collection (ATCC, Rockville, MD).

Three-dimensional porous PLLA and PLLA/GO scaffolds with 0.3%, 0.6%, 0.9%, and 1.2% GO were prepared by SLS. The powders were evenly laid on the sintering platform and selectively sintered according to the pre-planned scaffold models, and the sintering platform would be lowered to a corresponding height when a layer of powders was sintered and then a layer of powders was applied again, sintering layer by layer, and finally obtaining the required scaffolds. The processing parameters were applied as follows: Spot size of 1.2 mm, laser power of 2.2 W, and laser scanning speed of 100 mm/min.

### 2.2 Characterization

Surface and fracture morphologies were observed by Phenom Scanning Electron Microscopy (FEI Co., USA), and energy-dispersive spectroscopy (EDS) was used to examine the elemental content

of various substances. The phase composition of the scaffolds was carried out from 500 $cm^{-1}$ to 3500 $cm^{-1}$ with LabRAM HR800 confocal micro Raman spectrometer (HORIBA Scientific Instruments & Systems, Paris, France). Three-dimensional surface morphologies of PLLA/GO samples with 0%, 0.3%, 0.6%, 0.9%, and 1.2% GO after degradation for 4 weeks were observed by laser confocal microscopy (Zeiss Co., Germany) and surface roughness (Ra, Rq, and Rz) date was calculated automatically.

### 2.3 Wettability

The water contact angles of PLLA and PLLA/GO samples (10 × 10 × 5 $mm^3$) with 0.3%, 0.6%, 0.9%, and 1.2% GO were measured by an Attension Theta Lite optical tensiometer (Biolin Scientific Co. Ltd., Stockholm, Sweden). The water absorption of the samples was measured to determine the water uptake ability. Five times were used to measure the water absorption rate for each different ratio sample. The mass of each sample was weighed as $W_{dry}$ before immersing, and then the sample was immersed in the distilled water according to the pre-planned time and weighed as $W_{wet}$. The water absorption rate ($W_{war}$) was calculated by the following formula[43]:

$$W_{war} = \frac{W_{wet} - W_{dry}}{W_{dry}} \times 100\%$$

### 2.4 Degradation properties

Each sample with a size of 10 × 10 × 5 $mm^3$ was measured for initial weight as $W_i$ and then placed in a test tube containing 20 mL of PBS solution (pH = 7.4) at 37°. for 1, 2, 3, and 4 weeks, respectively. After reaching the predetermined immersing time, the samples were taken out and washed with distilled water 3 times, and then dried in a dry box for 24 h and weighted as $W_u$. The surface morphological changes were evaluated by SEM. The weight loss percentage ($W_L$) of the samples was calculated by the following formula[44]:

$$W_L = \frac{W_i - W_u}{W_i} \times 100\%$$

### 2.5 Mechanical properties

The mechanical properties of the samples were evaluated by a universal testing machine (WD-D1, LTD, China). Compressive samples were cylindrical scaffolds with 10 mm of diameter and 5 mm of height; tensile samples were dumbbell scaffolds with a size of 12 × 4 × 2 $mm^3$. Different proportions of the samples were placed on the compression fixture and subjected to uniaxial compression with a crosshead speed of 0.5 mm/min at room temperature. Similarly, the samples were also placed on the stretching fixture and subjected to uniaxial tensile under the same conditions. Compressive strength and modulus, tensile strength and modulus were calculated through stress-strain curves, respectively. Six samples were tested for each point.

### 2.6 Bioactivity

PLLA/GO samples (10 × 10 × 5 $mm^3$) with 0%, 0.3%, 0.6%, 0.9%, and 1.2% GO were placed in 6-well culture plates, immersed in 10 ml SBF, and maintained at 37°C. Fresh SBF was changed every other day for up to 4 weeks. After incubation for various periods of time, the specimens were removed from the solution and rinsed with deionized water 3 times to remove any soluble inorganic ions. Then, the samples were dried in a dry box for 24 h for further characterization.

### 2.7 Cytocompatibility

Fluorescence staining experiment was carried out to qualitatively assess the cell proliferation of PLLA and PLLA/0.9 GO scaffolds with a size of 10 × 10 × 5 $mm^3$. Twenty microliters of MTT solution were added into cell culture plates for 3 h at 37°C after 1, 3, and 5 days of cell culture. Subsequently, 200 mL of dimethyl sulfoxide was taken into each plate to dissolve formazan crystals and staining cells were imaged using a phase-contrast light microscope. The CCK-8 assay was used to quantificationally assess cell proliferation. The samples were cleaned with PBS after being cultured for 1, 3, and 5 days. Afterward, CCK-8 reagent (Dojindo Laboratories, Kumamoto, Japan) was added into culture plates and cultured

for 2 h. Finally, the absorbance of the solution was measured by a microplate reader at 450 nm.

### 2.8 Statistical analysis

Data were expressed as mean value ± one standard deviation. The differences of measured data were taken to be significant for $P < 0.05$, sign * and ** denotes $P < 0.05$ and $P < 0.01$, respectively.

## 3 Results and discussion

### 3.1 Preparation of powders and scaffolds

The morphology of the powders and scaffolds is shown in **Figure 1**. PLLA powders presented oblong or spherical particles in **Figure 1A**, and particle size was approximately 120 μm. In **Figure 1B**, GO presented flaky structure and piece of diameter was approximately 40 μm. PLLA/GO composites are shown in **Figure 1C**, GO was evenly distributed between PLLA particles, and the particle size was obviously smaller compared to PLLA particles. PLLA and PLLA/GO scaffolds were prepared by SLS, as shown in **Figure 1D-F**. PLLA scaffold presented a white appearance with a diameter of 12 mm and a height of 9 mm. Similarly, PLLA/GO had the same shape and size, while the appearance was grayish-black. More importantly, these scaffolds possessed interpenetrating micropores. These pores mimicked the microporous structure of bone, which facilitated the transport of nutrients, the discharge of metabolic waste, and the adhesion and proliferation of cells[45,46]. Feng *et al*. prepared three-dimensional porous structure scaffold and confirmed that the porous structure is favorable for cell growth[47].

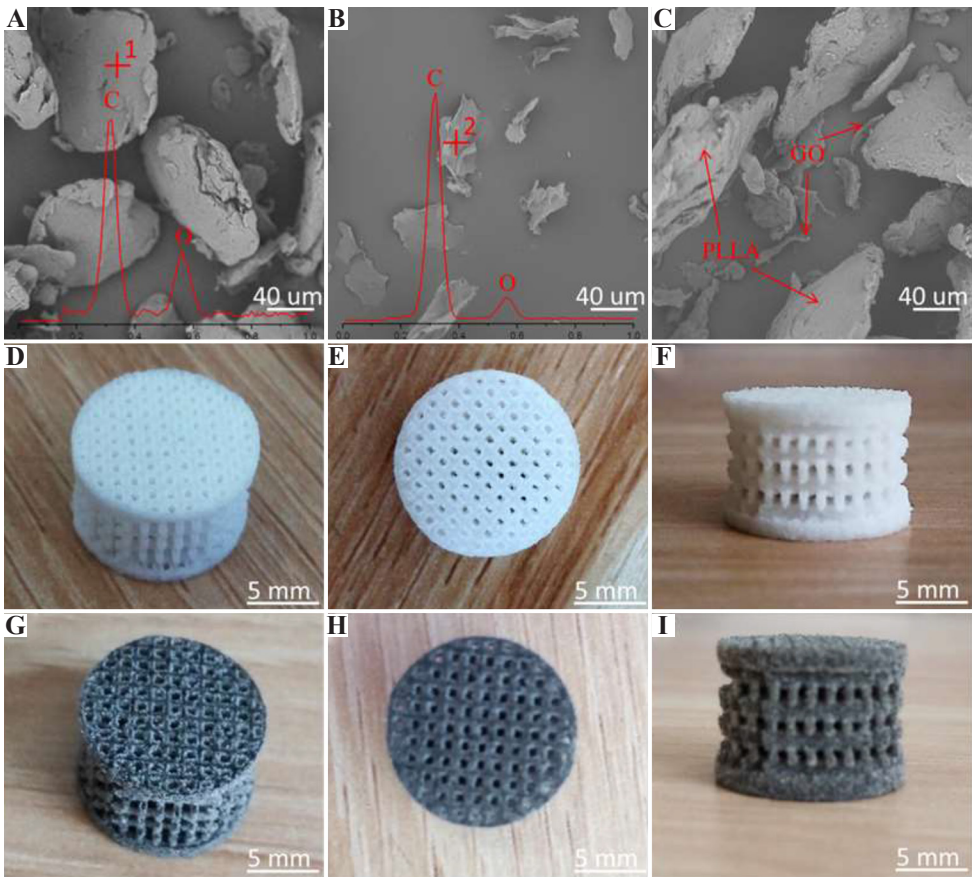


**Figure 1.** (A-C) SEM of PLLA, GO and PLLA/GO composite powders, (D-F) axis view, top view, and front view of the PLLA scaffold and (G-I) axis view, top view and front view of the PLLA/GO scaffold fabricated by SLS. PLLA and PLLA/GO scaffolds had similar shape sizes and interconnected porous structures.

### 3.2 Characterization

Raman spectroscopy was used to demonstrate the presence of GO in PLLA scaffolds and their interactions. As shown in **Figure 2A**, the Raman spectrum obtained for PLLA showed three obvious characteristic peaks at 871 $cm^{-1}$, 1451 $cm^{-1}$, and 2942 $cm^{-1}$. The PLLA/GO scaffold also showed three characteristic peaks in the same position. There were two new characteristic peaks appearing in the PLLA/GO spectra, representing the D (1330 $cm^{-1}$) and G (1544 $cm^{-1}$) peaks of GO, which confirmed the presence of GO in the PLLA matrix. To explore the interaction between PLLA and GO, the partial spectra in **Figure 2A** were magnified and showed, as shown in **Figure 2B**. The characteristic peaks at 1761 $cm^{-1}$ were C=O stretch of PLLA. Interestingly, the C=O peak shifted to high wavenumber when GO was introduced into the PLLA scaffold, demonstrating the possibly interaction between PLLA and GO because of hydrogen bonding. Geng *et al*. also reported a similar conclusion[48].

Water contact angle measurement was used to detect the hydrophilic properties of PLLA and PLLA/GO scaffolds with 0.3%, 0.6%, 0.9%, and 1.2% GO. The water contact angle of PLLA was 88.98°, which indicated that it had poor hydrophilic properties. The water contact angle began to decrease when GO was introduced. Water contact angle continuously decreased with increasing GO content, indicating that GO was beneficial to improve the hydrophilic properties of the PLLA scaffold. To further explore the

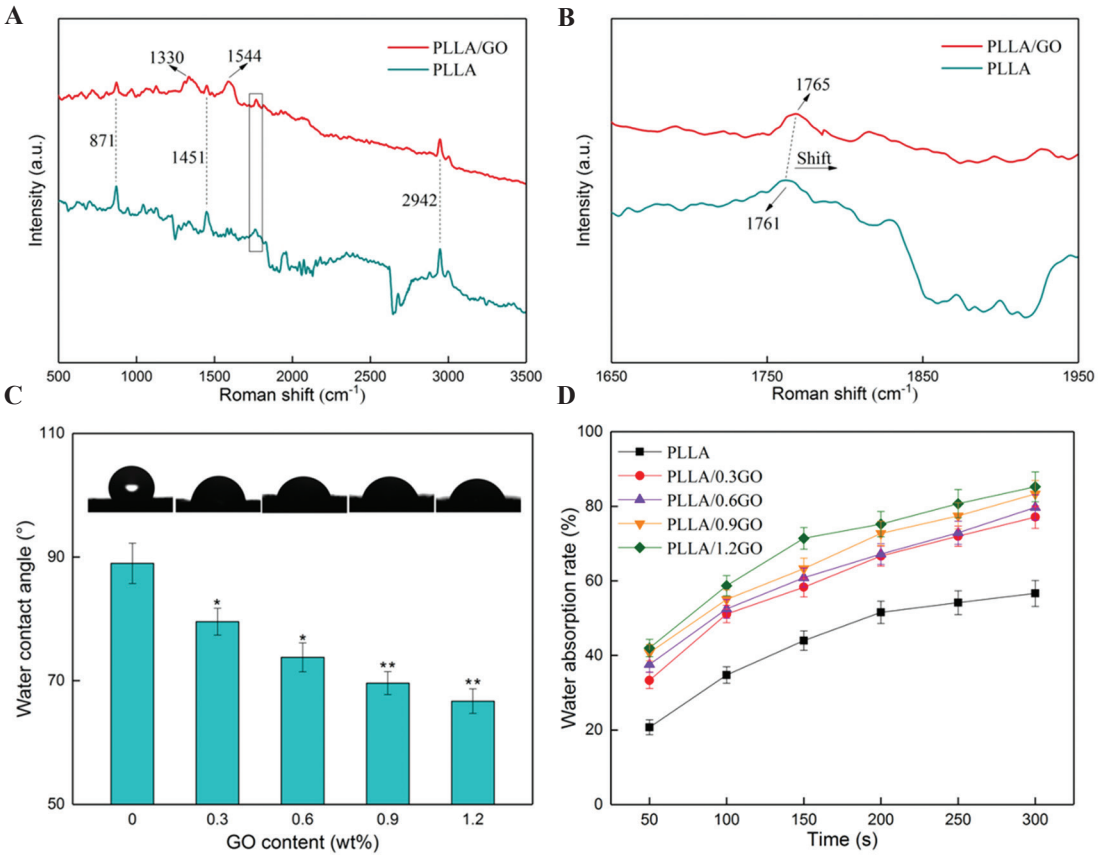


**Figure 2.** (A) Raman spectra of PLLA and PLLA/GO, and (B) partial magnification in spectra a. (C) Water contact angle of the PLLA scaffolds with 0%, 0.3%, 0.6%, 0.9%, and 1.2 wt % GO. (D) Water absorption rate of the PLLA scaffolds with 0%, 0.3%, 0.6%, 0.9%, and 1.2 wt % GO after immersing in aqueous solution for different time. GO was successfully introduced into the PLLA scaffold and interacted with PLLA. Hydrophilicity and water absorption capacity increased with increasing GO.

hydrophilic properties of scaffold, the water uptake of the scaffold was evaluated. The water absorption of the PLLA scaffold increased with the immersion time, while the slope of the increase in water absorption rate was decreased. Similarly, water absorption increased with the introduction of GO due to a large amount of hydrophilic groups on the surface of GO, which enhanced the water absorption capacity of scaffold.

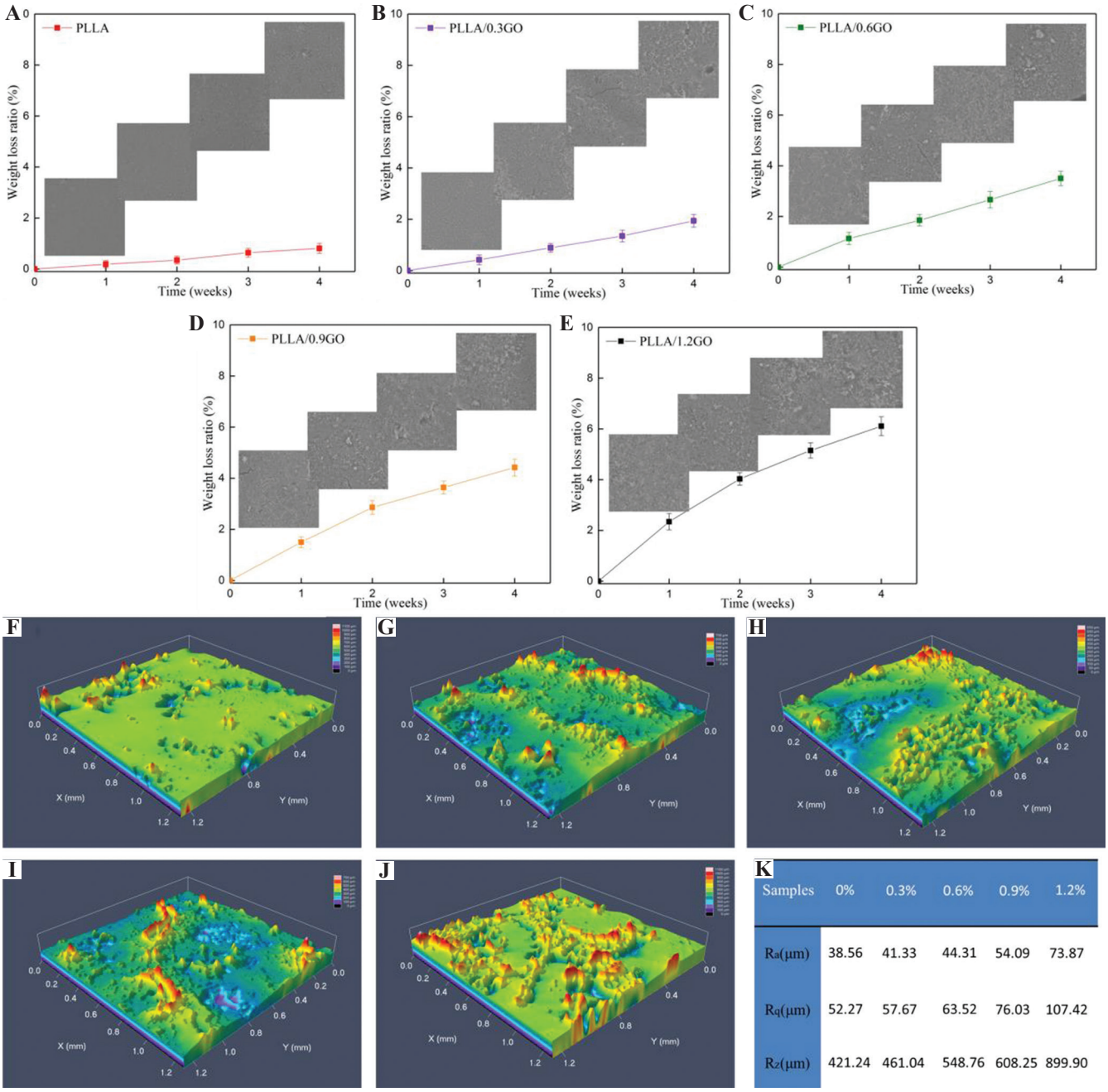


**Figure 3.** (A-E) The mass loss ratio and degradation morphology of PLLA scaffolds with 0%, 0.3%, 0.6%, 0.9%, and 1.2 wt % GO after immersing in PBS solution for 1, 2, 3, and 4 weeks, respectively. (F-J) Three-dimensional surface morphologies of PLLA/GO samples with 0%, 0.3%, 0.6%, 0.9%, and 1.2% GO after degradation for 4 weeks. (J) Surface roughness (Ra, Rq, and Rz) date of different ratios of PLLA/GO samples. Degradation of PLLA accelerated and surface roughness increased with increasing GO content.

### 3.3 Degradation properties

Degradation morphologies and mass loss of different proportions of PLLA/GO scaffolds are shown in **Figure 3A-E**. The surface of the PLLA sample did not change clearly after immersing in PBS for 1, 2, and 3 weeks (**Figure 3A**). When the immersing time was extended to 4 weeks, the surface of the sample became rough and surface roughness of Ra, Rq, and Rz was 38.56 μm, 52.27 μm, and 421.24 μm, respectively, and some precipitated particles appeared. Correspondingly, the mass loss of samples was measured to quantitatively assess the degree of degradation. It could be seen that PLLA had a small mass loss after 4 weeks of degradation and less than 1%. When 0.3% GO was introduced into PLLA, it could be seen that the surface of the PLLA/0.3 GO sample became rough after 1 week of soaking (**Figure 3B**). After 4 weeks of soaking, the surface began to appear degraded holes. As the GO content continued to increase, the surface of the samples became rougher and the quality loss also increased (**Figure 3C, D**). After soaking for 4 weeks, the surface of the PLLA/1.2 GO sample became rough with a Ra value of 73.87 μm, a Rq value of 107.42μm, and a Rz value of 899.90 μm and uneven, and the mass loss was close to 6%, indicating significant degradation and confirming that GO accelerated the degradation of PLLA (**Figure 3E**). Three-dimensional surface morphologies of PLLA/GO samples with 0%, 0.3%, 0.6%, 0.9%, and 1.2% GO after degradation for 4 weeks are shown in **Figure 3F-J**. It can be clearly seen that the surface of PLLA/GO samples after degradation became rougher as the GO content increased (**Figure 3K**).

### 3.4 Degradation mechanism

It was proved by the degradation of morphology and mass loss experiments that the introduction of GO could accelerate the degradation of PLLA. The explanation mechanism was also analyzed (**Figure 4**) as follows: First, the surface of GO contained a large number of oxygen-containing functional groups, and these functional groups had good hydrophilicity[49,50]. The introduction of GO

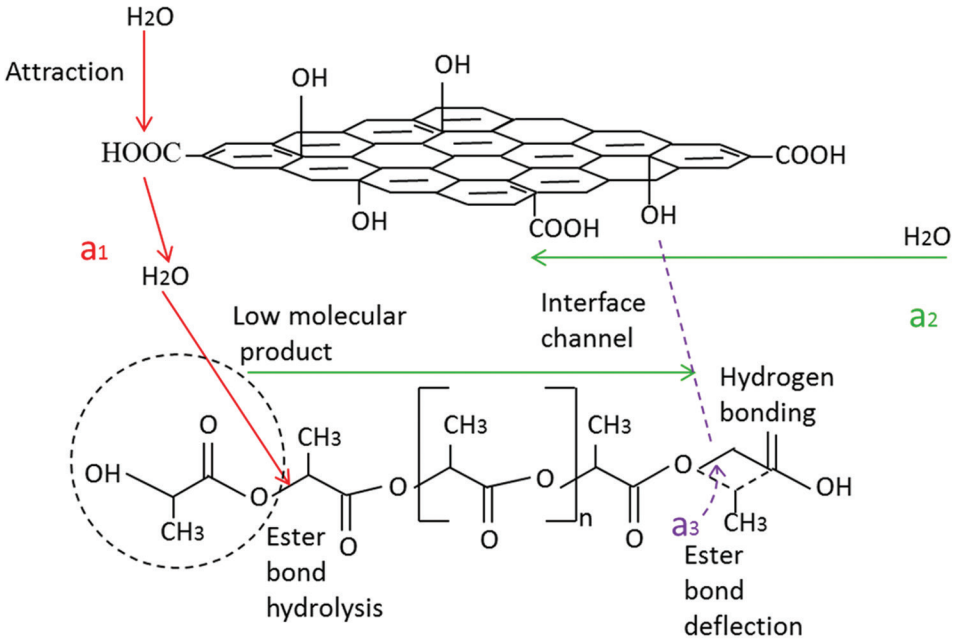


**Figure 4.** Schematic of GO promoting the degradation of PLLA. GO accelerated the degradation of PLLA could be divided into three parts. $a_1$: Hydrophilic GO attracted water molecules. $a_2$: The interface channels between GO and PLLA facilitated the intrusion of water molecules and discharged of degraded low molecular products. $a_3$: The hydrogen bonding between PLLA and GO induced the ester bond to deflect toward the interfaces, making the water molecules easily to attack the ester bond.

promoted the hydrophilic properties of the scaffold is demonstrated in **Figure 2**. Good hydrophilicity facilitated liquid intrusion into the scaffold. This process was described as $a_1$ and represented by the red line. Second, GO was a sheet-like structure with a large surface area and could form many interfaces with the PLLA matrix in the scaffold. These interfaces could be regarded as microchannels. On the one hand, the solution could enter the inside of the scaffold through the interface channels to promote the hydrolysis of ester bonds of the PLLA. On the other hand, these small molecule products produced by hydrolysis of the ester bond could also be discharged through the interface channels. This process was described as $a_2$ and was represented by the green line. Third, the oxygen-containing functional groups on the surface of GO could form hydrogen bond interaction with the ester bond of PLLA[51]. This interaction can induce the ester bond of PLLA to deflect toward the interface, promoting it be attacked by water molecules, thus accelerating the degradation of PLLA. This process was described as $a_3$ and was represented by the purple line.

### 3.5 Mechanical property

The compressive properties of samples containing different proportions of GO are presented in **Figure 5A and B**. The compressive strength of PLLA was 23.60 MPa, which was consistent with the report of Zhang[52]. The compressive strength was 37.51 MPa and increased by 58.9% when 0.3% GO was introduced. As the GO content continued to increase, the compressive strength gradually increased and reached a peak of 56.19 MPa when 0.9% GO was introduced. Nevertheless, when the content of GO increased from 0.9 wt% to 1.2 wt%, the compression strength of scaffolds decreased slightly from 56.19 MPa to 54.74 MPa. Similarly,

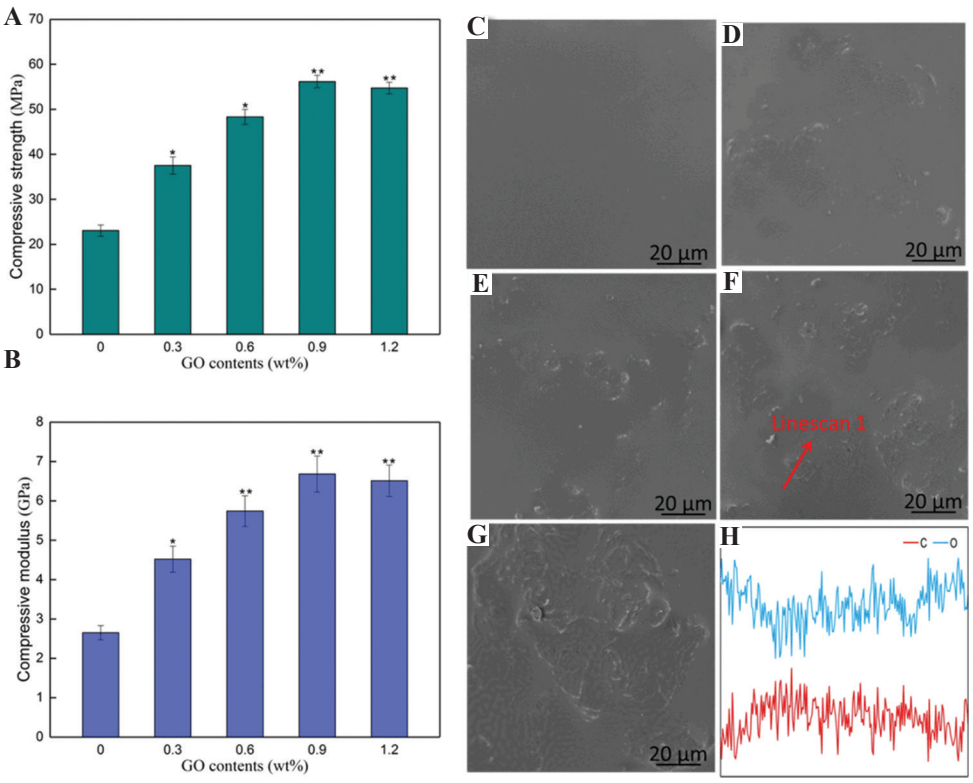


**Figure 5.** (A) Compressive strength and (B) compressive modulus of PLLA and PLLA/GO scaffolds with 0.3%, 0.6%, 0.9%, and 1.2 wt% GO. (C-G) Surface dispersion state of GO in PLLA substrate with 0%, 0.3%, 0.6%, 0.9%, and 1.2 wt% GO. (H) Linescan 1 showed the distribution of elements C and O. The compressive strength and modulus increased with increasing GO content, while there was a slight decrease when 1.2% GO was introduced. GO was uniformly dispersed in the PLLA matrix, but agglomerates formed when the GO content was further increased.

compression modulus also had a similar trend (**Figure 5B**). To investigate the cause of the change in compressive properties, the surface morphologies of the samples were observed by SEM, as shown in **Figure 5C-G**. The surface of PLLA was smooth and flat (**Figure 5C**), some flakes began to appear on the surface of the PLLA/0.3 GO sample (**Figure 5D**), and as the GO content continued to increase, more and more flakes appeared (**Figure 5E and F**). A large number of flakes were stacked together to form continuous agglomerates when 1.2% GO was introduced (**Figure 5G**). Red line scan 1 was used to distinguish the difference by penetrating the matrix and flakes (**Figure 5H**). In the direction of the line scan, the content of the C element first increased and then decreased. On the contrary, the content of the O element first decreased and then increased. The ratio of C to O elements proved that the flakes were GO. When the line scan 1 was moved from PLLA to GO, since the ratio of C to O in GO was higher than that of PLLA, so the C element rises. Then, when the line scan moved from GO to PLLA, the C element began to drop. The EDS of the powders in **Figure 1** also confirmed that the ratio of C to O in GO was larger than that in PLLA. The trend of the elements in the line scan 1 also confirmed that the flakes were GO. GO was a sheet-like structure with excellent mechanical strength, it could be used as a reinforcing phase to improve the compression properties of the scaffolds. However, when an excessive amount of GO was introduced, it was difficult to uniformly disperse and formed agglomerates, which formed defects in the matrix, resulting in a decrease in compressive strength.

The tensile strength and modulus of samples containing different GO ratios are measured and presented in **Figure 6A and B**. The tensile strength of PLLA was 16.90 MPa. As the GO content increased, the tensile strength also increased, but the tensile strength decreased when 1.2% GO was introduced. The compressive modulus was also increased first and then decreased. To explore the mechanism of tensile properties change, the fracture surface morphologies were analyzed by SEM. The fracture surface of PLLA was smooth with no obvious wrinkles, indicating that PLLA was brittle material (**Figure 6C**). Todo *et al*. also confirmed that the fracture mode of PLLA was brittle fracture[53]. When 0.3% GO was introduced, the fracture surface began to become rough and uneven (**Figure 6D**). GO sheets were embedded in the PLLA matrix when the content was increased to 0.6%, which was indicated by the red arrow (**Figure 6D**). When the GO content was further increased, more GO was embedded on the matrix, and the embedded GO could effectively transfer and consume external force, thereby increasing the tensile strength of the scaffolds. However, when the GO content was further increased, some of the GO sheets accumulated to form agglomeration, which weakened the enhancement of GO to PLLA, and thus the tensile strength and modulus decreased (**Figure 6G**).

### 3.6 Bioactivity

Good bioactivity is one of the required properties for bone scaffolds[54,55]. PLLA and PLLA/GO scaffolds with 0.3%, 0.6%, 0.9%, and 1.2 wt% GO were immersed in SBF for 4 weeks to assess bioactivity. There did not have a calcium-phosphorus layer appearing on the surface of PLLA after immersing in SBF, indicating that PLLA lacked good biological activity (**Figure 7A**). Zhou also has similar reports[56]. Calcium-phosphorus layer appeared on the surface of the sample when 0.3% GO was introduced into PLLA (**Figure 7B**). As the GO content continued to increase, there was more calcium-phosphorus layer on the surface of the sample, and the particle size was getting larger and larger (**Figure 7C-E**). Point 1 in **Figure 7E** was used to measure the elements of white particles by EDS, as shown in **Figure 7F**. There were Ca and P elements in the EDS map, which could prove that the white particles were the calcium-phosphorus layer. The surface of GO contained a large number of functional groups, such as –COOH and –OH[57-59]. These functional groups could adsorb Ca ions in SBF, and Ca ions could continue to adsorb $PO_4$ ions to nucleate and grow, thereby forming a calcium-phosphorus layer[60,61].

### 3.7 Cytocompatibility

Fluorescence staining experiment and CCK8 experiments were used to assess cell compatibility

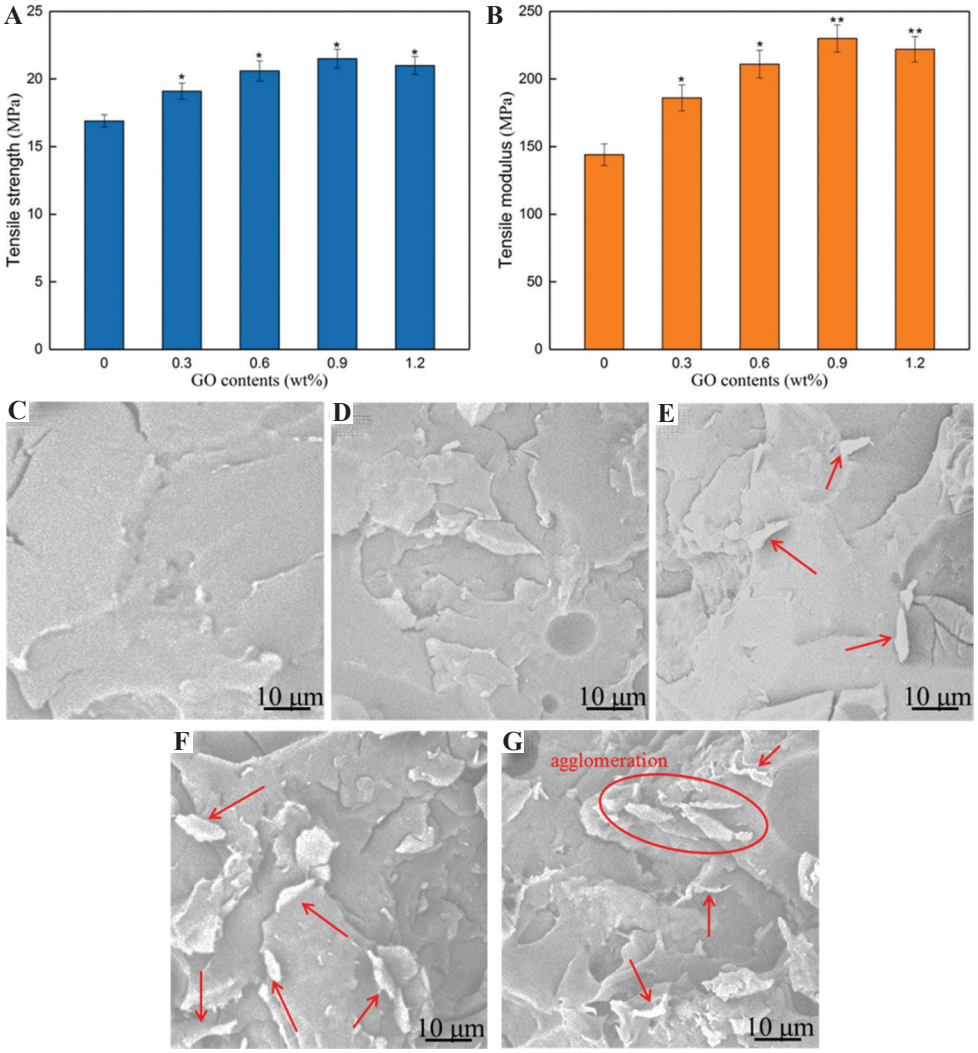


**Figure 6.** (A) Tensile strength and (B) tensile modulus of PLLA and PLLA/GO scaffolds with 0.3%, 0.6%, 0.9%, and 1.2 wt% GO. (C-G) Fracture morphology of GO in PLLA substrate with 0%, 0.3%, 0.6%, 0.9%, and 1.2 wt% GO. Tensile strength and modulus increased first and then decreased with increasing GO content. The fracture surface of PLLA was smooth, the introduction of GO rendered the fracture surface rough, and more GO was embedded in the PLLA matrix with the increase of GO.

by cultured on PLLA and PLLA/GO samples. MG63 cell was cultured on PLLA samples for 1 day, and the stained image is visualized in **Figure 8A**, living cells were dyed green by fluorescence, and showed spherical morphologies. The number of cells on PLLA/0.9 GO was more than that on PLLA after 1 day (**Figure 8B**). As the culture time of the cells on PLLA was extended, the number of cells was increasing (**Figure 8C and D**). After 5 days of culture, the cells on PLLA began to change from spherical to fusiform indicated by the red arrow. In contrast, cells on the PLLA/0.9 GO samples exhibited a more pronounced fusiform appearance compared to PLLA and covered almost the surface of the sample. CCK-8 experiment was used to qualitatively evaluate cytocompatibility. Compared to PLLA, the number of cells on PLLA/GO was higher than PLLA at any time (**Figure 8G**), indicating that the introduction of GO was beneficial to cell compatibility.

## 4 Conclusions

In this study, GO was introduced into PLLA to accelerate its degradation. PLLA/GO scaffolds were prepared by SLS and showed a three-dimensional

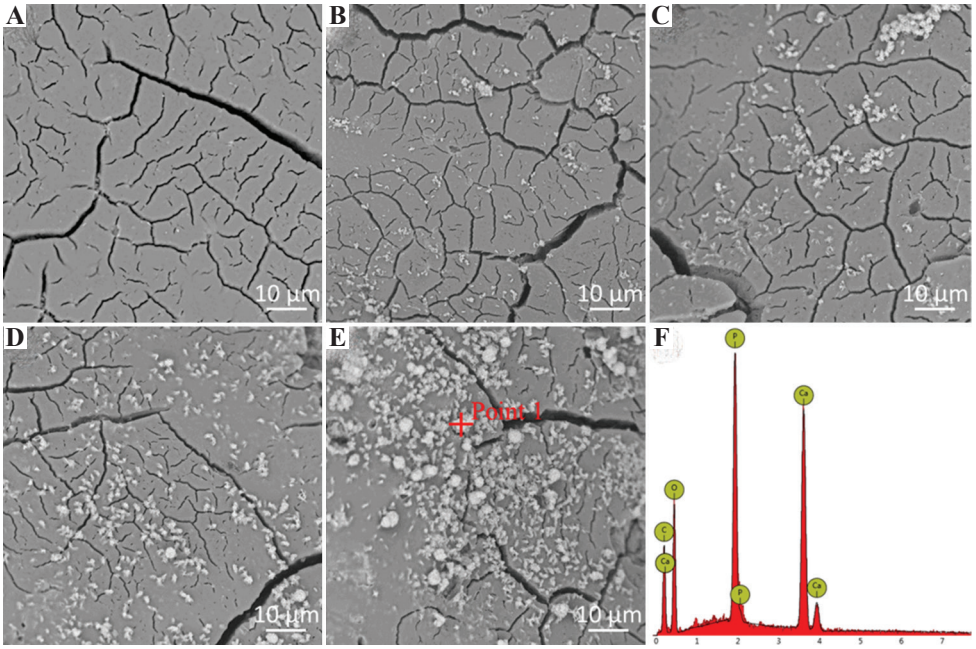


**Figure 7.** (A-F) Formation of a calcium-phosphorus layer of PLLA and PLLA/GO scaffolds with 0.3%, 0.6%, 0.9%, and 1.2 wt% GO after immersing in the SBF solution for 4 weeks. Samples containing GO possessed the ability of forming a calcium-phosphorus layer, while PLLA had no calcium-phosphorus layer formation.

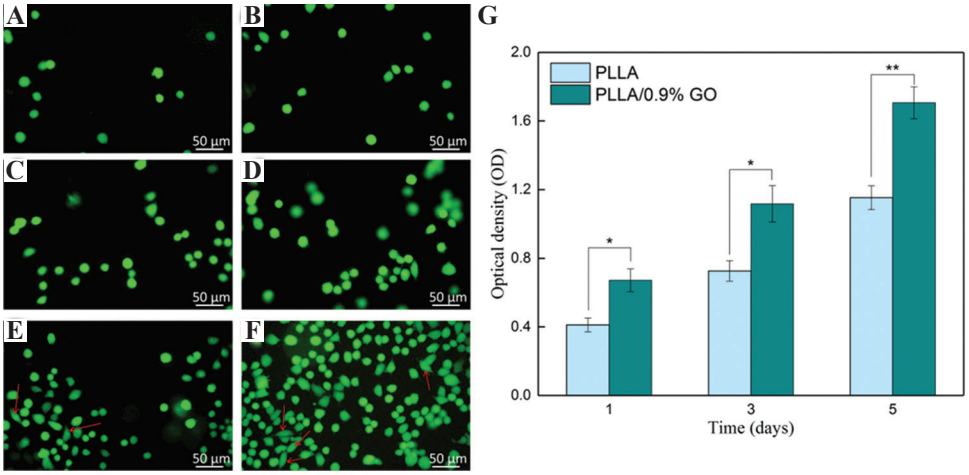


**Figure 8.** (A,C,E) The fluorescence staining of MG63 cells fostered on the PLLA scaffolds for 1, 3, and 5 days, (B,D,F) the fluorescence staining of MG63 cells fostered on the PLLA/0.9 GO scaffolds for 1, 3, and 5 days, respectively. (G) CCK-8 experiment of MG63 cells fostered on the PLLA and PLLA/0.9 GO scaffolds for 1, 3, and 5 days, respectively. Cells on PLLA/0.9 GO samples had better cell morphology and more cell number compared to PLLA.

porous structure. The introduction of GO increased the hydrophilicity and water absorption of the scaffolds, accelerated the breakage of the PLLA ester bonds. As a result, the surface of PLLA became rough and mass loss was increased from 0.81% to 6.11% after immersing for 4 weeks. Besides, the tensile strength was increased by 24.3% and compressive strength was also increased by 137.4%, respectively.

In addition, the scaffold also demonstrated good bioactivity and cytocompatibility. This study suggested that PLLA/GO scaffolds may be promising for bone tissue engineering.

## Acknowledgments

This work was supported by the following funds: (1) The Natural Science Foundation of China (51935014, 51905553, 81871494, 81871498, 51705540); (2) Hunan Provincial Natural Science Foundation of China (2019JJ50774, 2018JJ3671, 2019JJ50588); (3) JiangXi Provincial Natural Science Foundation of China (20192ACB20005); (4) Guangdong Province Higher Vocational Colleges & Schools Pearl River Scholar Funded Scheme (2018); (5) The Open-End Fund for the Valuable and Precision Instruments of Central South University; (6) National Postdoctoral Program for Innovative Talents (BX201700291); (7) The China Postdoctoral Science Foundation (2018M632983); (8) The Project of Hunan Provincial Science and Technology Plan (2017RS3008); (9) The Project of State Key Laboratory of High-Performance Complex Manufacturing, Central South University; and (10) The Fundamental Research Funds for the Central Universities of Central South University (2019zzts141, CX20190197).

## References

1. An J, Teoh JE, Suntornnond R, *et al.*, 2015, Design and 3D Printing of Scaffolds and Tissues. *Engineering*, 1:261–268.
2. Liu F, Mishbak H, Bartolo PJ, 2019, Hybrid Polycaprolactone/ Hydrogel Scaffold Fabrication and in-process Plasma Treatment Using PABS. *Int J Bioprint*, 5:174.
3. Cardoso, GB, Perea, GN, D'Avila, MA, *et al.*, 2011, Initial Study of Electrospinning PCL/PLLA Blends. *Adv Mater Phys Chem*, 1:94–98.
4. Saito Y, Minami K, Kobayashi M, *et al.*, 2002, New Tubular Bioabsorbable Knitted Airway Stent: Biocompatibility and Mechanical Strength. *J Thorac Cardiovasc Surg*, 123:161–167. DOI: 10.1067/mtc.2002.118503.
5. Shuai C, Yang W, He C, *et al.*, 2020, A Magnetic Micro-environment in Scaffolds for Stimulating Bone Regeneration. *Mater Des*, 185:108275. DOI: 10.1016/j.matdes.2019.108275.
6. Weng Y, Jin Y, Meng Q, *et al.*, 2013, Biodegradation Behavior of Poly (Butylene Adipate-co-terephthalate) (PBAT), Poly (Lactic Acid)(PLA), and their Blend under Soil Conditions. *Polym Test*, 32:918–926. DOI: 10.1016/j.polymertesting.2013.05.001.
7. Shuai C, Li Y, Feng P, *et al.*, 2019, Montmorillonite Reduces Crystallinity of Poly-l-lactic Acid Scaffolds to Accelerate Degradation. *Polym Adv Technol*, 30:2425–2435. DOI: 10.1002/pat.4690.
8. Tanaka M, Tanaka H, Hojo M, *et al.*, 2019, Change in Deformation/Fracture Behavior of Interface-controlled HAP/PLLA Composites by Hydrolysis, Proceedings of the 17th International Conference on Composite Materials, CD-ROM.
9. Yang Y, He C, Dianyu E, *et al.*, 2019, Mg Bone Implant: Features, Developments and Perspectives. *Mater Des*, 2019:108259.
10. Lee JH, Park TG, Park HS, *et al.*, 2003, Thermal and Mechanical Characteristics of Poly(L-lactic acid) Nanocomposite Scaffold. *Biomaterials*, 24:2773–2778. DOI: 10.1016/s0142-9612(03)00080-2.
11. Chen X, Wu X, Fan Z, *et al.*, 2018, Biodegradable Poly (Trimethylene carbonate-b-(L-lactide-ran-glycolide) Terpolymers with Tailored Molecular Structure and Advanced Performance. *Polym Adv Technol*, 29:1684–1696. DOI: 10.1002/pat.4272.
12. Shuai C, Yang Y, Feng P, *et al.*, 2018, A Multi-scale Porous Scaffold Fabricated by a Combined Additive Manufacturing and Chemical Etching Process for Bone Tissue Engineering. *Int J Bioprint*, 4:133. DOI: 10.18063/ijb.v4i1.133.
13. Shie MY, Fang HY, Lin YH, *et al.*, 2019, Application of Piezoelectric Cells Printing on Three-dimensional Porous Bioceramic Scaffold for Bone Regeneration. *Int J Bioprint*, 5:210. DOI: 10.18063/ijb.v5i2.210.
14. Yang Y, Wang G, Liang H, *et al.*, 2019, Additive manufacturing of bone scaffolds. *Int J Bioprint*, 5:184.
15. Ji JH, Park IS, Kim YK, *et al.*, 2015, Influence of Heat Treatment on Biocorrosion and Hemocompatibility of Biodegradable Mg-35Zn-3Ca Alloy. *Adv Mater Sci Eng*, 17:1–10. DOI: 10.1155/2015/318696.
16. Kang Y, Chen P, Shi X, *et al.*, 2018, Multilevel Structural Stereocomplex Polylactic Acid/collagen Membranes by Pattern Electrospinning for Tissue Engineering. *Polymer*, 156:250–260. DOI: 10.1016/j.polymer.2018.10.009.
17. Buwalda SJ, Dijkstra PJ, Calucci L, *et al.*, 2019, Influence of Amide versus Ester Linkages on the Properties of Eight-Armed PEG-PLA Star Block Copolymer Hydrogels. *Biomacromolecules*, 11:224–232. DOI: 10.1021/bm901080d.
18. Kontakis GM, Pagkalos JE, Tosounidis TI, *et al.*, 2007,

Bioabsorbable Materials in Orthopaedics. *Acta Orthop Belg*, 73:159–169.

19. Shuai C, Zan J, Yang Y, *et al*., 2019, Surface Modification Enhances Interfacial Bonding in PLLA/MgO Bone Scaffold. Mater Sci Eng C, 108:110486. DOI: 10.1016/j.msec.2019.110486.
20. Ding L, Wei Y, Wang Y, *et al.*, 2017, A Two-Dimensional Lamellar Membrane: MXene Nanosheet Stacks. *Angew Chem Int Ed Engl*, 56:1825–1829. DOI: 10.1002/anie.201609306.
21. Shen J, Hu Y, Shi M, *et al.*, 2009, Fast and Facile Preparation of Graphene Oxide and Reduced Graphene Oxide Nanoplatelets. *Chem Mater*, 21:3514–3520. DOI: 10.1021/cm901247t.
22. Wang G, Qi F, Yang W, *et al*., 2019, Crystallinity and Reinforcement in Poly-l-lactic Acid Scaffold Induced by Carbon Nanotubes. *Adv Polym Technol*, 2019:8625325.
23. Yoon OJ, Sohn IY, Kim DJ, *et al.*, Enhancement of Thermomechanical Properties of poly(D,L-lactic-co-glycolic acid) and Graphene Oxide Composite Films for Scaffolds. *Macromol Res*, 20:789–794. DOI: 10.1007/s13233-012-0116-0.
24. He S, Yang S, Zhang Y, Li X, *et al*., 2019, LncRNA ODIR1 Inhibits Osteogenic Differentiation of hUC-MSCs through the FBXO25/H2BK120ub/H3K4me3/OSX Axis. *Cell Death Dis*, 10:1–16. DOI: 10.1038/s41419-019-2148-2.
25. Depan D, Girase B, Shah JS, *et al.*, 2011, Structure-Process-Property Relationship of the Polar Graphene Oxide-mediated Cellular Response and Stimulated Growth of Osteoblasts on Hybrid Chitosan Network Structure Nanocomposite Scaffolds. *Acta Biomater*, 7:3432–3445. DOI: 10.1016/j.actbio.2011.05.019.
26. Xiong G, Luo H, Zuo G, *et al.*, Novel Porous Graphene Oxide and Hydroxyapatite Nanosheets-reinforced Sodium Alginate Hybrid Nanocomposites for Medical Applications. *Mater Charact*, 107:419–425. DOI: 10.1016/j.matchar.2015.07.016.
27. Chen J, Shi X, Ren L, *et al.*, 2016, Graphene Oxide/PVA Inorganic/Organic Interpenetrating Hydrogels with Excellent Mechanical Properties and Biocompatibility. *Carbon*, 111:18–27. DOI: 10.1016/j.carbon.2016.07.038.
28. Zhao X, Zhang Q, Chen D, *et al.*, 2010, Enhanced Mechanical Properties of Graphene-Based Poly(vinyl alcohol) Composites. *Macromolecules*, 44:2392–2392. DOI: 10.1021/ma200335d.
29. Wang K, Ruan J, Song H, *et al.*, 2011, Biocompatibility of Graphene Oxide. *Nanoscale Res Lett*, 6:1–8.
30. Gao C, Yao M, Shuai C, *et al.*, 2019, Nano-SiC Reinforced Zn Biocomposites Prepared via Laser Melting: Microstructure, Mechanical Properties and Biodegradability. *J Mater Sci Technol*, 35:2608–2617. DOI: 10.1016/j.jmst.2019.06.010.
31. Rodríguez-Lozano FJ, García-Bernal D, Aznar-Cervantes S, *et al.*, 2014, Effects of Composite Films of Silk Fibroin and Graphene Oxide on the Proliferation, Cell Viability and Mesenchymal Phenotype of Periodontal Ligament Stem Cells. *J Mater Sci Mater Med*, 25:2731–2741. DOI: 10.1007/s10856-014-5293-2.
32. Li W, Xu Z, Chen L, *et al.*, 2014, A Facile Method to Produce Graphene Oxide-g-poly (L-lactic acid) as an Promising Reinforcement for PLLA Nanocomposites. *Chem Eng J*, 237:291–299. DOI: 10.1016/j.cej.2013.10.034.
33. Zhang K, Zheng H, Liang S, *et al.*, 2016, Aligned PLLA Nanofibrous Scaffolds Coated with Graphene Oxide for Promoting Neural Cell Growth. *Acta Biomater*, 37:131–142. DOI: 10.1016/j.actbio.2016.04.008.
34. Pan LH, Kuo SH, Lin TY, *et al.*, 2017, An Electrochemical Biosensor to Simultaneously Detect VEGF and PSA for Early Prostate Cancer Diagnosis Based on Graphene Oxide/ssDNA/PLLA Nanoparticles. *Biosens Bioelectron*, 89:598–605. DOI: 10.1016/j.bios.2016.01.077.
35. Chen Q, Mangadlao JD, Wallat J, *et al.*, 2017, 3D Printing Biocompatible Polyurethane/Poly (Lactic Acid)/Graphene Oxide Nanocomposites: Anisotropic Properties. *ACS Appl Mater Interfaces*, 9:4015–4023. DOI: 10.1021/acsami.6b11793.
36. Yuan S, Shen F, Chua CK, *et al.*, 2019, Polymeric Composites for Powder-based Additive Manufacturing: Materials and Applications. *Prog Polym Sci*, 91:141–168. DOI: 10.1016/j.progpolymsci.2018.11.001.
37. Lee JY, An J, Chua CK, 2017, Fundamentals and Applications of 3D Printing for Novel Materials. *Appl Mater Today*, 7:120–133.
38. Zhuang P, Sun AX, An J, *et al.*, 2018, 3D Neural Tissue Models: From Spheroids to Bioprinting. *Biomaterials*, 154:113–133. DOI: 10.1016/j.biomaterials.2017.10.002.
39. Mir TA, Iwanaga S, Kurooka T, *et al.*, 2019, Biofabrication Offers Future Hope for Tackling Various Obstacles and Challenges in Tissue Engineering and Regenerative Medicine: A Perspective. *Int J Bioprint*, 5:153. DOI: 10.18063/ijb.v5i1.153.
40. Ng WL, Chua CK, Shen YF, 2019, Print me an Organ! Why we are not there yet. *Prog Polym Sci*, 97:101145. DOI: 10.1016/j.progpolymsci.2019.101145.
41. Lee JM, Sing SL, Zhou M, *et al.*, 2018, 3D Bioprinting Processes: A Perspective on Classification and Terminology. *Int J Bioprint*, 4:151. DOI: 10.18063/ijb.v4i2.151.

42. Zhuang P, Ng WL, An J, *et al.*, 2019, Layer-by-Layer Ultraviolet Assisted Extrusion-based (UAE) Bioprinting of Hydrogel Constructs with High Aspect Ratio for Soft Tissue Engineering Applications. *PLoS One*, 14:e0216776. DOI: 10.1371/journal.pone.0216776.
43. Lins LC, Wianny F, Livi S, *et al.*, Development of Bioresorbable Hydrophilic-hydrophobic Electrospun Scaffolds for Neural Tissue Engineering. *Biomacromolecules*, 17:3172–3187. DOI: 10.1021/acs.biomac.6b00820.
44. Gao C, Yao M, Li S, *et al.*, 2019, Highly Biodegradable and Bioactive Fe-Pd-Bredigite Biocomposites Prepared by Selective Laser Melting. *J Adv Res*, 20:91–104. DOI: 10.1016/j.jare.2019.06.001.
45. Wei G, Ma PX, 2004, Structure and Properties of Nano-Hydroxyapatite/Polymer Composite Scaffolds for Bone Tissue Engineering. *Biomaterials*, 25:4749–4757. DOI: 10.1016/j.biomaterials.2003.12.005.
46. Xia W, Chang J, 2010, Bioactive Glass Scaffold with Similar Structure and Mechanical Properties of Cancellous Bone. *J Biomed Mater Res Part B Appl Biomater*, 95:449–455. DOI: 10.1002/jbm.b.31736.
47. Feng P, Kong Y, Yu L, *et al.*, 2019, Molybdenum Disulfide Nanosheets Embedded with Nanodiamond Particles: Co-dispersion Nanostructures as Reinforcements for Polymer Scaffolds. *Appl Mater Today*, 17:216–226. DOI: 10.1016/j.apmt.2019.08.005.
48. Geng LH, Peng XF, Jing X, *et al.*, Investigation of Poly(l-lactic acid)/Graphene Oxide Composites Crystallization and Nanopore Foaming Behaviors via Supercritical Carbon Dioxide Low Temperature Foaming. *J Mater Res*, 31:348–359. DOI: 10.1557/jmr.2016.13.
49. Morales-Narváez E, Baptista-Pires L, Zamora-Gálvez A, *et al.*, 2017, Graphene-Based Biosensors: Going Simple. *Adv Mater*, 29:1604905. DOI: 10.1002/adma.201604905.
50. Kaniyoor A, Baby TT, Ramaprabhu S, 2010, Graphene Synthesis via Hydrogen Induced Low Temperature Exfoliation of Graphite Oxide. *J Mater Chem*, 20:8467–8460. DOI: 10.1039/c0jm01876g.
51. Eckhart KE, Holt BD, Laurencin MG, *et al.*, 2019, Covalent Conjugation of Bioactive Peptides to Graphene Oxide for Biomedical Applications. *Biomater Sci*, 7:3876–3885. DOI: 10.1039/c9bm00867e.
52. Zhang P, Wang BT, Gao D, *et al.*, The Study on the Mechanical Properties of Poly (Lactic Acid)/Straw Fiber Composites. *Appl Mech Mater*, 2012:312–315.
53. Todo M, Park SD, Arakawa K, *et al.*, 2006, Relationship between Microstructure and Fracture Behavior of Bioabsorbable HA/PLLA Composites. *Compos Part A Appl Sci Manuf*, 37:2221–2225. DOI: 10.1016/j.compositesa.2005.10.001.
54. Yang Y, He C, Dianyu E, *et al.*, 2019, Mg Bone Implant: Features, Developments and Perspectives. *Mater Des*, 185:108259. DOI: 10.1016/j.matdes.2019.108259.
55. Shuai C, Liu G, Yang Y, *et al.*, 2020, Functionalized $BaTiO_3$ Enhances Piezoelectric Effect towards Cell Response of Bone Scaffold. *Colloids Surf B Biointerfaces*, 185:110587. DOI: 10.1016/j.colsurfb.2019.110587.
56. Zhou Z, Liu L, Liu Q, *et al.*, 2012, Effect of Surface Modification of Bioactive Glass on Properties of Poly-L-Lactide Composite Materials. *J Macromol Sci Part B*, 51:1637–1646. DOI: 10.1080/00222348.2012.672295.
57. Alexa A, Rahnenführer J, Lengauer TR, 2006, Improved Scoring of Functional Groups from Gene Expression Data by Decorrelating GO Graph Structure. *Bioinformatics*, 22:1600–1607. DOI: 10.1093/bioinformatics/btl140.
58. Shuai C, Cheng Y, Yang Y, *et al.*, 2019, Laser Additive Manufacturing of Zn-2Al Part for Bone Repair: Formability, Microstructure and Properties. *J Alloys Compd*, 798:606–615. DOI: 10.1016/j.jallcom.2019.05.278.
59. Yang X, Li X, Ma X, *et al.*, 2014, Carbonaceous Impurities Contained in Graphene Oxide/Reduced Graphene Oxide Dominate their Electrochemical Capacitances. *Electroanalysis*, 26:139–146. DOI: 10.1002/elan.201300128.
60. Wang H, Zhao S, Xiao W, *et al.*, 2016, Influence of Cu Doping in Borosilicate Bioactive Glass and the Properties of its Derived Scaffolds. *Mater Sci Eng C*, 58:194–203. DOI: 10.1016/j.msec.2015.08.027.
61. Suntornnond R, An J, Chua CK, 2017, Roles of Support Materials in 3D Bioprinting-Present and Future. *Int J Bioprint*, 3:321–328. DOI: 10.18063/ijb.2017.01.006.